Orientation of plastic rearrangements in two-dimensional model glasses under shear

Alexandre Nicolas*
LPTMS, CNRS, Univ. Paris-Sud, Université Paris-Saclay, 91405 Orsay, France

Jörg Rottler†
Department of Physics and Astronomy and Quantum Matter Institute, University of British Columbia, Vancouver BC V6T 1Z1, Canada

(Received 11 February 2018; published 11 June 2018)

The plastic deformation of amorphous solids is mediated by localized shear transformations involving small groups of particles rearranging irreversibly in an elastic background. We introduce and compare three different computational methods to extract the size and orientation of these shear transformations in simulations of a two-dimensional athermal model glass under simple shear. We find that the shear angles are broadly distributed around the macroscopic shear direction, with a more or less Gaussian distribution with a standard deviation of around 20°. The distributions of sizes and orientations of shear transformations display no substantial sensitivity to the shear rate. These results can notably be used to refine the description of rearrangements in elastoplastic models.

DOI: 10.1103/PhysRevE.97.063002

I. INTRODUCTION

Polydisperse foams, highly concentrated emulsions, molecular glasses, and bulk metallic glasses exhibit microscopically heterogeneous mechanical properties. As a result, these disordered solids do not deform affinely under shear. Instead, their deformation features bursty rearrangements of small groups of particles embedded in an otherwise elastically deforming medium. It is now well accepted that these microscopically localized shear transformations (ST) are the elementary carriers of plastic deformation in sheared amorphous solids [1,2]. By straining its surroundings, each ST gives rise to a characteristic long-range deformation halo around it [3,4], which mediates most collective effects in the material, such as cascades of rearrangements [5,6].

Based on this picture at the particle scale, mesoscale elastoplastic models of amorphous plasticity have been formulated, which divide the material into small regions (blocks) that are loaded elastically until they fail plastically [7]. The failure of a block is described as an ideal ST which partly dissipates the local stress and partly redistributes it to the other blocks. For an ST in d-dimensional space, the Green's function $\mathcal{G}$ for the nonlocal redistribution of the shear stress satisfies

$$\mathcal{G}(r,\theta) \simeq C\cos[4\theta + 2\theta^{\mathrm{pl}}]/r^d \qquad (1)$$

in the plane of the transformation, with a dimension-dependent prefactor C, where (r,θ) are the polar coordinates in the frame centered on the plastic block and θ^{pl} [defined precisely in Eq. (3)] refers to the orientation of the individual ST. The far-field limit of this expression for $\mathcal{G}$ matches Eshelby's solution for a spherical inclusion endowed with a spontaneous strain [8] and was shown to suitably describe the disorder-averaged response of an amorphous solid to an ideal ST in atomistic simulations [9].

Mesoscale models, however, rest on several assumptions concerning the STs, including their idealized "Eshelby" nature, their equal size, and their orientation along the direction of maximal local shear [10,11] or even along the macroscopic shear direction in scalar models [12,13] (in this regard, Ref. [14] is an exception). To give them stronger footing, experimental and numerical efforts have been made to characterize plastic rearrangements, as exposed in Sec. II. In particular, much attention has been paid to their shape and their size [1,15–17], while the question of their orientation has remained largely unexplored, despite its obvious relevance for the buildup of spatial correlations between individual STs [18,19]. In this contribution, we simulate the shear deformation of a two-dimensional (2D) athermal model glass (described in Sec. III) with molecular dynamics in order to study the statistical properties of actual rearrangements for different shear rates. Strong emphasis is placed on their angles of failure. To this end, we propose (in Sec. III) and compare (in Sec. V) several numerical methods to extract these angles. We find that these angles are broadly distributed around the macroscopic shear direction, with a more or less Gaussian distribution with a standard deviation of around 20°. Overall, the sizes and orientations of the detected rearrangements are fairly insensitive to the shear rate, but many of them actually differ from ideal STs. Even when the ideal ST description works reasonably well, local methods relying exclusively on the displacements (or forces) of the most active rearranging particles give poor estimates of the ST orientation; the latter is recovered if a broader selection of particles near the ST is considered.

II. PREVIOUS ENDEAVORS TO CHARACTERIZE PLASTIC REARRANGEMENTS

Leaving aside Schwarz's early attempts to classify rearrangements in a 3D foam at rest [20], Argon and Kuo were

*alexandre.nicolas@polytechnique.edu
†jrottler@physics.ubc.ca

the first to report localized rearrangements in a disordered system, more precisely a 2D foam ("bubble raft") that was used as a model system for metallic glasses [1]. Interestingly, they mentioned two types of STs: sharp slips of rows of about five bubbles in length and more diffuse cooperative rearrangements of regions of five bubbles in diameter. In the 1980s, Princen studied the swap of neighbors between four bubbles (in 2D) to account for some rheological properties of foams and concentrated emulsions [21]; the detailed dynamics of this swap process were investigated much later in clusters of four bubbles [22]. In slowly sheared colloidal glasses, STs were directly visualized using confocal microscopy and their core was observed to be around three particle diameters in linear size [15]. In metallic glasses, direct visualization of STs cannot be achieved experimentally but estimates for their volumes can be obtained indirectly (e.g., via nanoindentation tests and their sensitivity to the shear rate) and typically correspond to a few dozen atoms (∼30 in the Zr-based glass studied with nanoindentation tests in Ref. [23]), with a possible dependence on the sample morphology (for instance, for a Ni-Nb metallic glass, the ST size was reported to decrease from 83 atoms to 36 atoms when the material was cast into a μm-thin film [16]).

Numerically, the most comprehensive characterization of rearrangements to date was performed by Albaret *et al.* [17] on a 3D atomistic model for amorphous bulk silicon under quasistatic shear. Rearrangements were detected by artificially reverting the applied strain increments at every step and deducing the irreversible changes that took place; the detected rearrangements were then modeled as a collection of Eshelby inclusions, whose sizes (or volumes V_0) and eigenstrains $\boldsymbol{\epsilon}^\star$ were fitted to best reproduce the displacement field measured during the actual strain increment. These inclusions were shown to account for all plastic effects visible in the stress-strain curves of these materials and the effective volume $\gamma^\star V_0$ (where $\gamma^\star$ is the maximal shear component of $\boldsymbol{\epsilon}^\star$) was found to be exponentially distributed, with a typical size of 70 Å^3, while both dilational and contractional volumetric strains were observed. The evolution of the effective volume $\gamma^\star V_0$ during the transformation was computed in Ref. [24] by detecting the saddle point; the value of the effective volume at this saddle point, called activation volume, was found to amount to around 20% of the final $\gamma^\star V_0$.

III. NUMERICAL MODEL AND METHODS

A. Model and simulation protocol

In order to get information on the morphology and orientation of STs, we perfom molecular dynamics simulations of an amorphous material (a glass) under simple shear, in 2D and in the athermal limit. The model glass is a binary mixture of A and B particles, with $N_A = 32500$ and $N_B = 17500$, of respective diameters $\sigma_{\rm AA} = 1.0$ and $\sigma_{\rm BB} = 0.88$, confined in a square box of dimensions $205\sigma_{\rm AA} \times 205\sigma_{\rm AA}$, with periodic boundary conditions. The system, at density 1.2, was prepared by quenching an equilibrated configuration at temperature $T = 1$ with a fast quenching rate $\dot{T} = 2 \times 10^{-3}$, at constant volume. The particles, of mass $m = 1$, interact via a pairwise Lennard-Jones potential,

$$V_{\alpha\beta}(r) = 4\epsilon_{\alpha\beta}\left[\left(\frac{\sigma_{\alpha\beta}}{r}\right)^{12} - \left(\frac{\sigma_{\alpha\beta}}{r}\right)^{6}\right],$$

where $\alpha,\beta = A, B$, $\sigma_{AB} = 0.8$,$\epsilon_{\rm AA} = 1.0$, $\epsilon_{AB} = 1.5$, and $\epsilon_{\rm BB} = 0.5$. The potential is truncated at $r = 2.5\sigma_{\rm AA}$ and shifted for continuity. Simple shear γ is imposed at rate $\dot{\gamma}$ by deforming the (initially square) box into a parallelogram and remapping the particle positions. After an initial transient (20% strain), the system reaches a steady state, which is the focus of the present study.

In the athermal limit, the equations of motion read

$$\frac{dr_i}{dt} = v_i; \quad m\frac{dv_i}{dt} = -\sum_{i\neq j}\frac{\partial V(r_{ij})}{\partial r_{ij}} + f_i^D.$$

The dissipative force f_i^D experienced by particle i is computed with a dissipative particle dynamics scheme, viz.,

$$f_i^D = -\sum_{j\neq i}\zeta\, w^2(r_{ij})\frac{v_{ij}\cdot r_{ij}}{r_{ij}^2}r_{ij}$$

$$\text{where } w(r) \equiv \begin{cases} 1-\frac{r}{r_c} & \text{if } r < r_c \equiv 3\sigma_{\rm AA}, \\ 0 & \text{otherwise.} \end{cases} \qquad (2)$$

Here $v_{ij} \equiv v_i - v_j$ denotes the relative velocity of particle i with respect to j, $r_{ij} \equiv r_i - r_j$, and $\zeta = 1/\tau_{\rm LJ}$ controls the damping intensity (the effect of the damping was studied in Ref. [25]). Equations (2) are integrated with the velocity Verlet algorithm with a time step $dt = 0.005$. In all the following, we use $\tau_{\rm LJ} \equiv \sqrt{m\sigma_{\rm AA}^2/\epsilon}$ as the unit of time and $\sigma_{\rm AA}$ as the unit of length.

B. Detection of rearrangements

As expected, the simulations display fast localized rearrangements. Several measures are available to identify them and are known to yield comparable results [26]. In Fig. 1, we compute three of these diagnostics of nonaffinity on a typical snapshot of a simulation at shear rate $\dot{\gamma} = 10^{-4}$. These diagnostics are based on the displacements δu_j of particles j during a short time interval $[t, t+\delta t]$, with $\delta t = 2$. Figure 1(a) shows the amplitude of the minimized mean-square difference

$$d^2_{\rm min} = \min_{\boldsymbol{G}}\sum_{r_j\in\mathcal{C}}[\delta u_j - \delta u_0 - \boldsymbol{G}\cdot(r_j - r_0)]^2$$

between the actual displacements δu_j of particles j in a circular region $\mathcal{C}$ around a given particle r_0 and *any* set of affine displacements, i.e., displacements resulting from a uniform displacement gradient $\boldsymbol{G}$ during δt [2]. This measure of the nonaffine residual strain has become a quasi gold standard for identifying plastic rearrangements in amorphous solids. Figure 1(b) shows a simpler measure, namely the amplitude of the average kinetic energy of a particle averaged over δt. The motivation is that in an athermal system, only particles undergoing a rearrangement are expected to have large marginal velocities. Lastly, in Fig. 1(c) we consider the magnitudes of the (linearized) forces $f_i^{(\mathcal{H})} = -\sum_j \boldsymbol{\mathcal{H}}_{ij}(t)\cdot\delta u_j$, where $\boldsymbol{\mathcal{H}}_{ij}(t) = \frac{\partial^2 V}{\partial r_i r_j}$ is the Hessian matrix at time t. These are the forces that effectively drive plastic rearrangements. As discussed by Lemaître [19], they also localize in regions of high nonaffine strain.

Figure 1 confirms that the three methods give very similar results. Accordingly, for convenience, we choose to use a

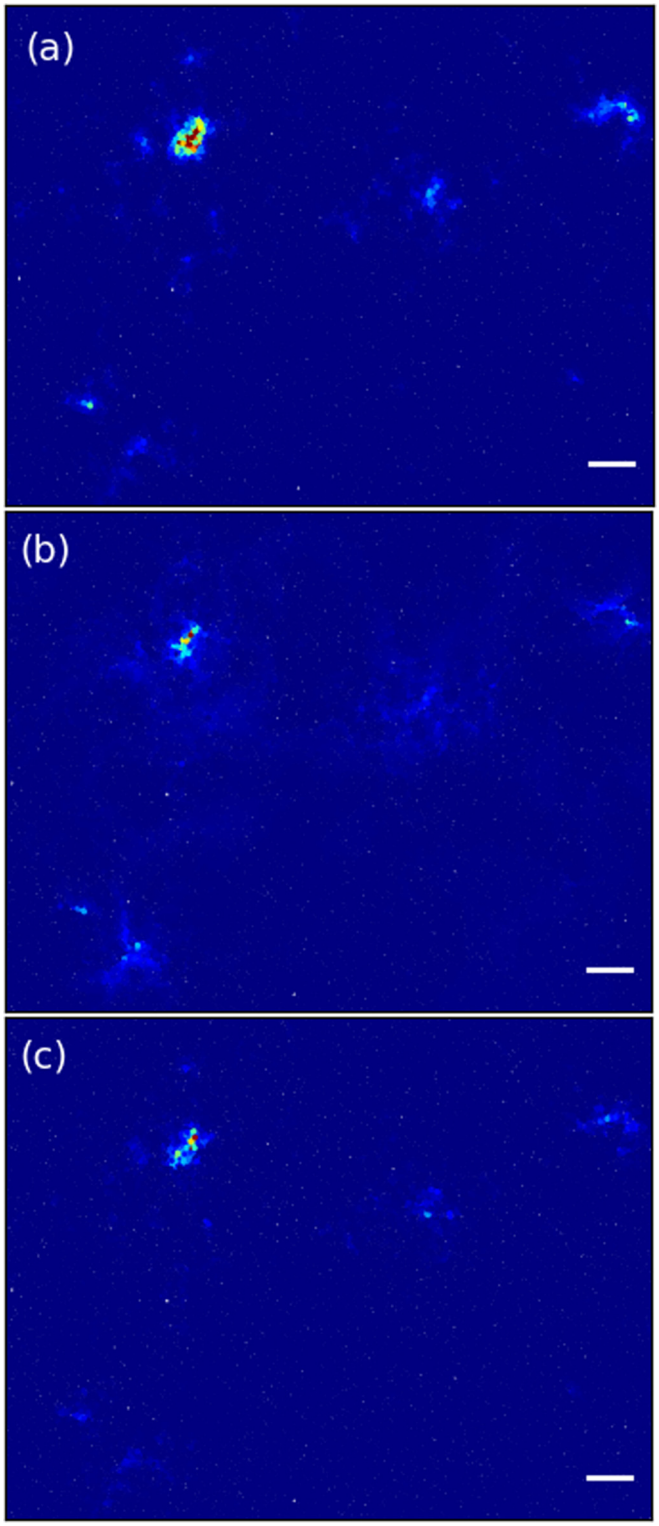

FIG. 1. Detection of plastic events via (a) the $d^2_{\min}$ criterion, (b) by the average kinetic energy of a particle, and (c) the magnitude of the linearized "Hessian" forces (see text). The scale bar is 10 particle diameter.

criterion based on kinetic energies to detect rearrangements. More precisely, particles with a kinetic energy larger than an arbitrary threshold $e_{\min}$ are considered to be rearranging; the threshold value is lowered to $^3/_4\, e_{\min}$ for the neighbors

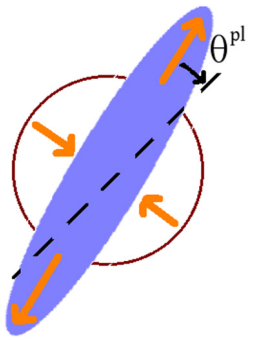

FIG. 2. Representation of the angle of failure $\theta^{\rm pl}$. The orange arrows indicate the elongational and contractional directions of an ideal ST, while the dashed line represents the elongational direction of the macroscopic shear.

of rearranging particles, in order to obtain more compact ST shapes, where two particles are defined as neighbors if they are separated by a distance smaller than 2. Finally, rearranging particles are partitioned into clusters of neighbors, each corresponding to an individual ST (clusters with fewer than three particles were discarded). The distributions $p(S)$ of sizes of the resulting clusters for distinct thresholds $e_{\min}$ and distinct shear rates $\dot\gamma$ are represented in Fig. 3; neither the threshold nor the shear rate seem to considerably alter the seemingly slower-than-exponential (but faster-than-power-law) decay of $p(S)$. In the following, we shall see that all our results are fairly insensitive to these parameters $e_{\min}$ and $\dot\gamma$. We have also checked (though inexhaustively) that the distributions of orientations of rearrangements detected on the basis of the linearized forces $f_i^{(\mathcal{H})}$ are compatible with those shown below.

C. Methods to measure ST orientations

In order to study ST orientations, a rearrangement is likened to a circular Eshelby inclusion with an eigenstrain $\boldsymbol{\epsilon}^\star$, i.e., a region whose stress-free state is not reached for a deformation $\boldsymbol{\epsilon}(r) = \mathbf{0}$ but for $\boldsymbol{\epsilon}(r) = \boldsymbol{\epsilon}^\star$ (if it were unconstrained). The eigenstrain $\boldsymbol{\epsilon}^\star$ can be split into a deviatoric part, associated with shape change, and a volumetric part, associated with local dilation, viz.,

$$\boldsymbol{\epsilon}^\star = \epsilon^\star \begin{pmatrix} \sin 2\theta^{\rm pl} & \cos 2\theta^{\rm pl} \\ \cos 2\theta^{\rm pl} & -\sin 2\theta^{\rm pl} \end{pmatrix} + \epsilon_v \begin{pmatrix} 1 & 0 \\ 0 & 1 \end{pmatrix} \qquad (3)$$

with $\epsilon^\star \geqslant 0$. We define the ST orientation as the *angle of failure* $\theta^{\rm pl} \in]-90^\circ, 90^\circ]$; it is thus the angle between the elongational principal direction of the ST and that of the macroscopic shear, as sketched in Fig. 2.

1. Fit to an Eshelby inclusion

We are now left with the problem of determining $\boldsymbol{\epsilon}^\star$ in practice. Drawing inspiration from Albaret *et al.* [17], we exploit the elastic field induced by an inclusion à la Eshelby. For homogeneous isotropic elastic media, the deformation $\boldsymbol{\epsilon}^{\rm in}$ within any embedded elliptical inclusion will be constant. It naturally follows that, for a circular inclusion, the principal directions of $\boldsymbol{\epsilon}^{\rm in}$ and $\boldsymbol{\epsilon}^\star$ will be identical due to symmetry arguments. Outside the circular inclusion (of radius a and

centered at $r = 0$), the induced displacements δu are given by [27]

$$\begin{aligned}\delta u_1(r) &= \frac{x_1}{8(1-\nu)}\tilde{a}^2\{[2(1-2\nu)+\tilde{a}^2](\epsilon_{11}-\epsilon_{22})+2\tilde{a}^2(\epsilon_{11}+\epsilon_{22})+4(1-\tilde{a}^2)(\tilde{x}_1^2\epsilon_{11}+\tilde{x}_2^2\epsilon_{22})\}\\ &+\frac{x_2}{8(1-\nu)}\tilde{a}^2 2\epsilon_{12}[2(1-2\nu)+\tilde{a}^2+4(1-\tilde{a}^2)\tilde{x}_1^2]\\ \delta u_2(r) &= \frac{x_2}{8(1-\nu)}\tilde{a}^2\{[2(1-2\nu)+\tilde{a}^2](\epsilon_{22}-\epsilon_{11})+2\tilde{a}^2(\epsilon_{11}+\epsilon_{22})+4(1-\tilde{a}^2)(\tilde{x}_1^2\epsilon_{11}+\tilde{x}_2^2\epsilon_{22})\}\\ &+\frac{x_1}{8(1-\nu)}\tilde{a}^2 2\epsilon_{12}[2(1-2\nu)+\tilde{a}^2+4(1-\tilde{a}^2)\tilde{x}_2^2],\end{aligned} \tag{4}$$

where $r = (x_1, x_2)$ and tildes denote distances rescaled by the norm of r (viz., $\tilde{x}_1 = x_1/r$).

For each rearranging cluster, the equivalent size a and eigenstrain components $\epsilon^\star$, ϵ_v, and $\theta^{\rm pl}$ defined in Eq. (3) are calculated as the parameters minimizing the squared difference between the particle displacements $\delta u_i'$ over $\delta t = 2$ and the theoretical expectations of Eq. (4), for all particles i that are at a distance between $2a$ and a large distance $d_{\max}$ away from the cluster center; the quality of the fit will be measured by the relative squared difference χ^2. (Note that the results turned out to be insensitive to the value of $d_{\max}$.) However, unlike Ref. [17], the displacements $\delta u_i'$ are not extracted from the actual dynamical simulation. Instead, in order to avoid the superposition of many STs, we run an auxiliary simulation

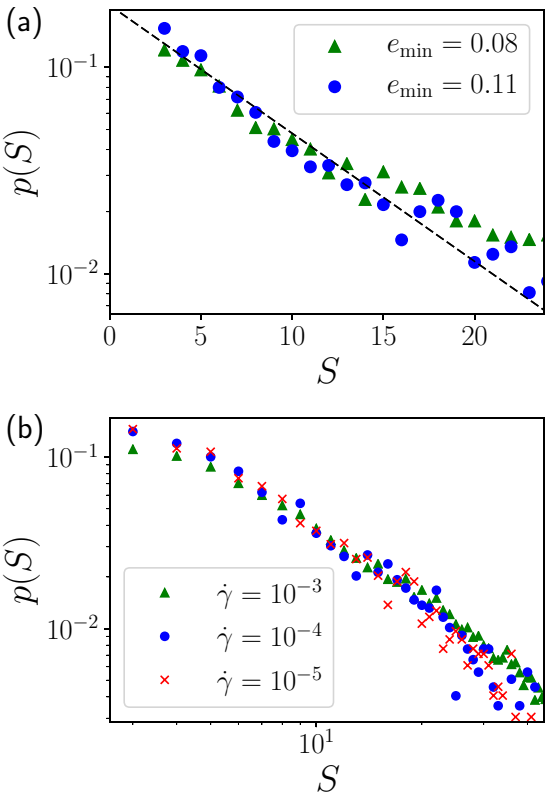

FIG. 3. Distribution of sizes S of the rearranging clusters detected with the kinetic energy based criterion (a) for two different threshold values $e_{\min}$ at $\dot\gamma = 10^{-5}$ and (b) for three different shear rates $\dot\gamma$ with $e_{\min} = 0.11$. The thin dashed line in the top panel is proportional to $\exp(-S/S_0)$ with $S_0 = 7$.

for each rearranging cluster so as to measure the response induced only by this cluster. Pragmatically, starting from the configuration at t, we move particles j belonging to the cluster by a fraction $\alpha \ll 1$ of their actual displacements δu_j, pin them to their new positions, and obtain the response $\alpha\delta u_i'$ of the other particles to this local rearrangement by minimization. This strategy, which we refer to as MD/Esh, will be our main method to access the ST morphology. One should nevertheless be aware that the results of the auxiliary simulations display a slight sensitivity to the details of the minimization procedure, but the consistency of our results will prove that this sensitivity can be overlooked.

2. *Azimuthal modes of the displacements induced by the STs*

A variant of this method may save us the cost of the fitting step. As mentioned in the introduction, the strain field $\boldsymbol{\delta\epsilon}$ induced by the shear part ($\epsilon^\star$) of an ST has a fourfold azimuthal symmetry. Therefore, focusing on $\delta\epsilon_{xy}$ for instance, the $m = 4$ azimuthal mode of $\delta\epsilon_{xy}(r)$ contains all information pertaining to the ST orientation (whereas the $m = 2$ component results from the dilational part ϵ_v). In practice, using the auxiliary simulations described above, we compute the local strain around each particle (i.e., the tensor $\boldsymbol{\delta\epsilon}_i$ which minimizes the local nonaffine deviations $d^2_{\min}$ introduced in Sec. III B), coarse-grain the xy-shear strain field into boxes of linear size $r_c = 3$ (see Fig. 4), and compute the azimuthal Fourier modes c_m of the resulting coarse-grained field $\delta\epsilon^c_{xy}$ along a circle of radius r (much larger than the cluster size), viz.,

$$c_m = \int_0^{2\pi} e^{-{\rm i}m\theta}\delta\epsilon^c_{xy}(r,\theta)d\theta. \tag{5}$$

Calculating c_4 for the quadrupolar strain field and writing it as $c_4 = |c_4|e^{{\rm i}\phi_4}$, we find that the angle of failure is related to ϕ_4 via $\theta^{\rm pl} = \phi_4/2$. We call this method MD/azi.

3. *Methods exclusively based on the forces or displacements of rearranging particles*

The two methods described above involve minimization steps and/or additional (auxiliary) simulations and are therefore numerically costly. To bypass this cost, we will try to get information on the ST by using only the observed displacements δu_i of the particles i within the rearranging cluster. A first idea is to compute the internal part $\boldsymbol{\sigma}$ of the local stress tensor: $\boldsymbol{\sigma} = -V^{-1}\sum_i f_i \otimes r_i$, where V is the cluster size, the sum runs over all particles i in the cluster, each subjected to an average force f_i and undergoing a displacement

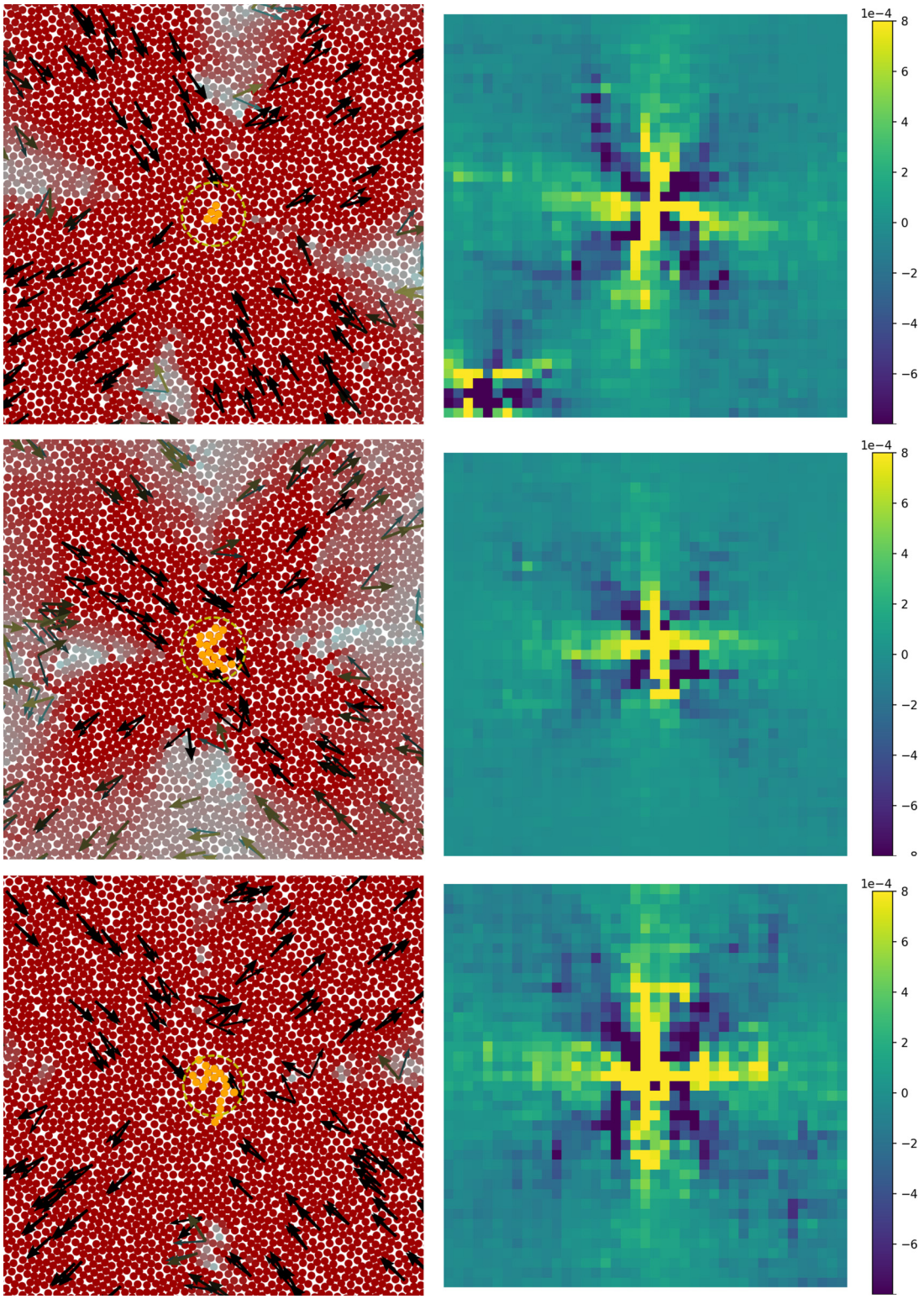

FIG. 4. Elastic reponse computed in the auxiliary MD simulations (see text) to a selection of three STs exhibiting a quadrupolar response. In the left column, particles in the ST are colored in orange, while the colors of the other particles depend on the norms of their displacements δu_i (warmer colors denote larger displacements). The arrows with wide shafts represent the directions of δu_i for a random subset of particles, while the (directions of) displacements represented by narrower arrows are the response to the best-fitting Eshelby inclusion. The figures shown are zooms on a 50×50 portion of the global system (of size 205×205). The right column presents the coarse-grained strain field $\delta\epsilon^c_{xy}$ computed from the associated auxiliary simulations, in a 100×100 square around the cluster.

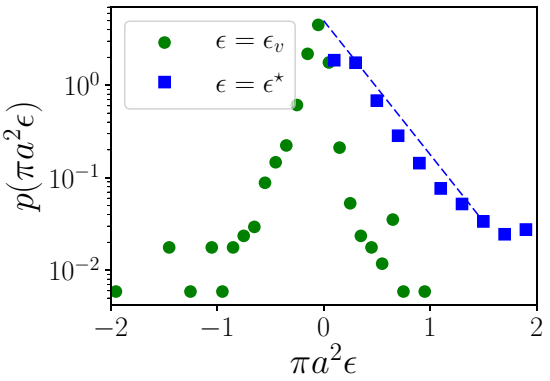

FIG. 5. Distribution of the dilational strengths $\pi a^2 \epsilon_v$ (circles) and the shear strengths $\pi a^2 \epsilon^\star$ (squares) of the STs detected at $\dot{\gamma} = 10^{-5}$ (with threshold $e_{\min} = 0.11$). The dashed blue line is proportional to $\exp(-x/0.3)$.

δu_i between t and $t + \delta t$. The analog for the displacements is the tensor $\mathcal{M} = -V^{-1} \sum_i \delta u_i \otimes r_i$. Positions r_i are expressed relative to the cluster centers of gravity, and the mean force (or displacement) among the ST particles is drawn off the f_i (or u_i). A yield angle $\theta^{\rm pl}$ can be extracted from these tensors by symmetrising them and writing their deviatoric (traceless) part $\boldsymbol{s}^{\rm dev}$ as

$$\boldsymbol{s}^{\rm dev} = -\alpha \begin{pmatrix} \sin 2\theta^{\rm pl} & \cos 2\theta^{\rm pl} \\ \cos 2\theta^{\rm pl} & -\sin 2\theta^{\rm pl} \end{pmatrix}, \tag{6}$$

with a coefficient $\alpha > 0$ (the minus sign comes from the sign convention used to define the Cauchy stress). These methods will be referred to as Loc. We have checked that they yield the same result as the inspection of the azimuthal mode c_4 of the response of an isotropic homogeneous elastic *continuum* to the set of pointwise forces $F_i = f_i$, or $F_i \propto \delta u_i$ for the displacement-based version, as computed by means of the Oseen-Burgers tensor. (We have underlined the word *continuum* to insist on the difference with the MD/azi method).

IV. CHARACTERISTICS OF STS

In this section, we employ the method based on fitting rearranging clusters to Eshelby inclusions in order to unveil key characteristics of the rearrangements. Although STs are often idealized as pure shear transformations, the volumetric deformations are found not to be negligible in practice. In Fig. 5, we report the distributions of the dilational strengths $\pi a^2 \epsilon_v$ and the shear strengths $\pi a^2 \epsilon^\star$ of the STs detected at $\dot{\gamma} = 10^{-5}$, where πa^2 is the surface of the inclusion and ϵ_v and $\epsilon^\star$ were defined in Eq. (3). The corresponding plots at $\dot{\gamma} = 10^{-4}, 10^{-3}$ are very similar. As in Ref. [17], we observe an exponential distribution of shear strengths, with a typical value around 0.3 here. One should, however, note that, since the present simulations are not quasistatic, the detected rearrangements (computed over $\delta t = 2$) often do not cover the whole transformation, which lasts for several time units.

Moving on to the ST orientations, we plot the distribution $p(\theta^{\rm pl})$ of angles of failure obtained at the three shear rates in Fig. 6(a). We observe no significant sensitivity to the shear rate. Besides, the central part of $p(\theta^{\rm pl})$ can be approximated

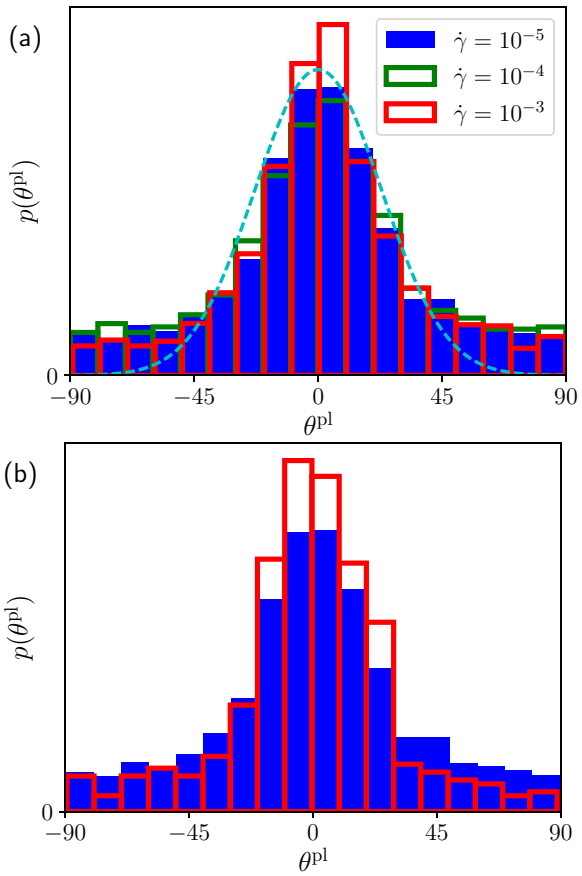

FIG. 6. Distributions of angles of failure $\theta^{\rm pl}$ obtained with the MD/Esh method. (a) Comparison of $p(\theta^{\rm pl})$ between distinct shear rates $\dot{\gamma}$. The dashed line represents a normal distribution with standard deviation $\delta\theta^{\rm pl} = 23^\circ$. (b) Distribution $p(\theta^{\rm pl})$ at $\dot{\gamma} = 10^{-5}$ before (filled blue) and after (red) removing the STs which substantially deviate from their Eshelby fits ($\chi^2 > 0.5$).

by a normal distribution with standard deviation $\delta\theta^{\rm pl} = 23^\circ$, but $p(\theta^{\rm pl})$ has heavier tails. If we discard the STs for which the elastic response significantly deviates from the Eshelby fit [Fig. 6(b)], the peak of $p(\theta^{\rm pl})$ sharpens slightly, but this does not strongly affect its shape.

It is interesting to compare these results with those predicted by a mainstream tensorial elastoplastic model in simple shear [28]. The latter also showed a Gaussian-like distribution $p(\theta^{\rm pl})$ which was virtually insensitive to the shear rate, but which was by far narrower than the present ones, with standard deviations of 3–4° that could increase up to ≈7° if cooperativity in the flow was enhanced by increasing the duration of plastic events or if elasto-plastic blocks were advected along the flow, instead of being static (see chap. 9.2, p. 111, of Ref. [28]). In these models, angular deviations from the macroscopic shear direction $\theta^{\rm pl} = 0$ are exclusively due to cooperative effects, whereby the stress redistributed during an ST [Eq. (1)] may load other blocks along a direction $\theta^{\rm pl} \neq 0$, depending on their relative positions. The much broader distribution $p(\theta^{\rm pl})$ measured in the present atomistic simulations hints at the impact of the granularity of the local medium, which may favor failure along a direction distinct from that of the local loading.

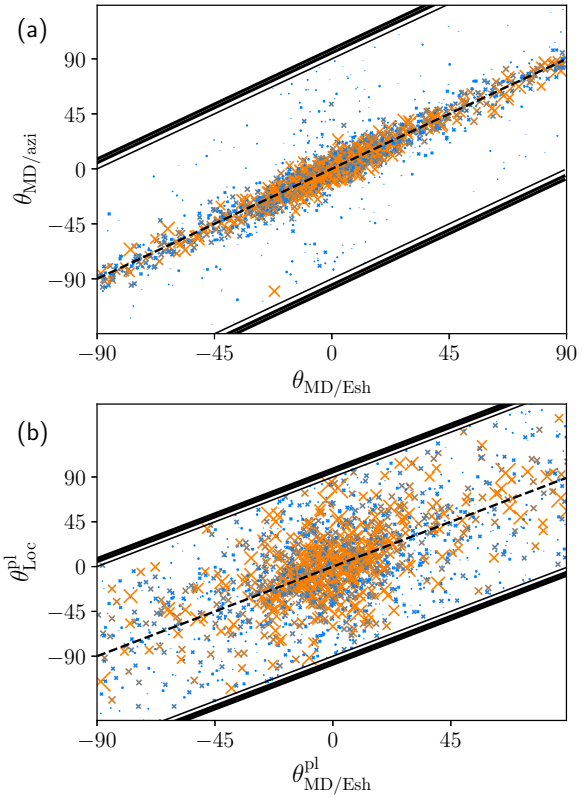

FIG. 7. Scatter plot of angles of failure θ^{pl} measured at $\dot{\gamma} = 10^{-5}$ with (a) the MD/Esh method vs. the MD/azi method and (b) the MD/Esh method vs. the displacement-based Loc method. Large (orange) crosses refer to STs with good Eshelby fits, while small (blue) crosses indicate poor fits; more precisely, the sizes of the crosses are inversely proportional to the χ^2 deviation from the fit.

V. COMPARISON BETWEEN DISTINCT METHODS TO MEASURE ST ORIENTATIONS

Having characterized the strengths and orientations of STs, we now discuss to what extent the ST characteristics can be extracted from methods that do not rely on fits to Eshelby inclusions.

A. Azimuthal mode of the induced strain

We start by considering the MD/azi method introduced in Sec. III C 2, which extracts the quadrupolar azimuthal mode of the xy strain (from the auxiliary MD simulations) on a circle of radius r to determine θ^{pl}. The angles of failure θ^{pl} measured at distinct r ($r = 17$ and $r = 23$) are typically within $\pm 10^\circ$ of one another (data not shown); there are outliers, but these very generally correspond to STs that strongly deviate from the Eshelby fits. Hereafter, we fix the radius at $r = 17$. Figure 7(a) shows that the individual MD/azi angles of failure agree relatively well with those determined with the MD/Esh method used so far, with absolute differences smaller than 20° for STs with reasonable Eshelby fits.

B. Methods based on local forces or displacements

Turning to the results obtained with local methods (Sec. III C 3), we report that we have not found any correlation between the MD/Esh angles of failure and those determined with force-based local methods, whether it be the total force f_i or the "linearized" forces $f_i^{(\mathcal{H})}$ (both being averaged over δt). On the other hand, displacement-based local methods broadly agree with MD/Esh, even though this does not immediately transpire from the scatter plot of Fig. 7(b). To prove the overall consistency of the methods despite this large noise, we split the detected STs into 10°-wide bins depending on their orientation $\theta^{\mathrm{pl}}_{\mathrm{MD/Esh}}$ and, for each bin, plot the average angle $\theta^{\mathrm{pl}}_{\mathrm{Loc}}$ (measured with the displacement-based local method) in Fig. 8. On a technical note, one should mention that, to average over angles $\theta_1, \ldots, \theta_n$, we computed the circular average $\arg(\sum_j e^{\mathbf{i}\theta_j})$. With these averaged data, the two methods are found to be in good accordance [29].

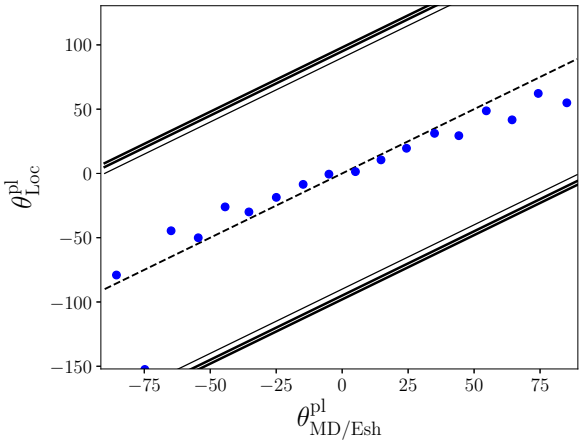

FIG. 8. Comparison between the angles of failure $\theta^{\mathrm{pl}}_{\mathrm{MD/Esh}}$ and $\theta^{\mathrm{pl}}_{\mathrm{Loc}}$ measured with the MD/Esh method and the displacement-based local method, respectively. The STs have been binned into 10°-wide angular windows, according to the value of $\theta^{\mathrm{pl}}_{\mathrm{MD/Esh}}$.

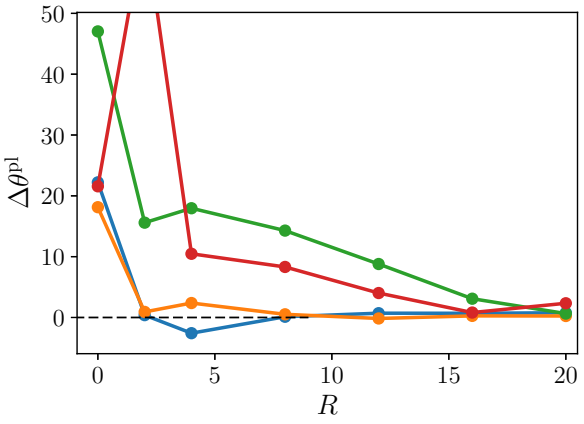

FIG. 9. Differences $\Delta\theta^{\mathrm{pl}}$ between the angles of failure found with the local method based on the displacements of all particles within a distance R of the ST center of gravity (in the auxiliary simulation) and the MD/Esh method for four STs that displayed good Eshelby fits ($\chi^2 < 1$) but large discrepancies with the Loc method. For $R = 0$, the local method makes only use of the rearranging particles as identified by the kinetic energy threshold.

To shed light on the discrepancies in the one-to-one comparison, we extend the local method by including the displacements (measured in the auxiliary simulation) of all particles within a distance R of the center of gravity of the ST, instead of only the rearranging particles, with the expectation that both methods converge when $R \to \infty$. In Fig. 9, we apply this method to STs detected at $\dot{\gamma} = 10^{-5}$ for which a mismatch between $\theta^{\mathrm{pl}}_{\mathrm{Loc}}$ and $\theta^{\mathrm{pl}}_{\mathrm{MD/Esh}}$ was observed, despite fairly good fits to Eshelby inclusions. The figure suggests a reasonably quick convergence between the two methods, although the radii R at which convergence is reached strongly depend on the ST. This implies that the deficiency of the pristine Loc method stems from its biased selection of too few particles for the computation of the local tensor.

VI. CONCLUSION

This paper has introduced and compared three approaches to extract the size and orientation of STs in sheared amorphous solids. Rearranging particles were grouped into clusters based on a threshold criterion for the kinetic energy, which is reliable for athermal solids, and their displacements over a small time interval were recorded. Once these clusters are extracted, auxiliary simulations are performed in which the particles taking part in a given ST are displaced and the remainder is relaxed via energy minimization. In the first approach, which we consider to be the most general one, the resulting displacment field is then analyzed by fitting to the ideal "Eshelby" solution for the far-field displacements. In the second method, this fitting is avoided by instead computing the azimutal mode of the (coarse grained) strain field resulting from the ST. Angles of failure obtained from these two methods agree well with each other as long as the Eshelby fit itself is reasonable.

A third and purely local method that avoids auxiliary simulations altogether consists in computing the deviatoric part of the displacement (inertia) tensor after the rearranging clusters have been identified. These angles of failure agree less well with those from Eshelby fits in a point by point comparison, but can be shown to be overall consistent after the noise is reduced through averaging. The inclusion of a larger number of particles improves the agreement between the methods considerably. In practice, this extended local method is the most efficient one as long as the STs do not overlap.

It will be interesting to compare the angles of failure of STs to the local configurations *prior to* failure, in particular the direction of the maximal shear stress and the directional dependence of the local yield stress, which can be measured by deforming a small region embedded in a purely affinely deforming region [30,31]. Moreover, our results suggest that mesoscopic elastoplastic models [7] should be refined to better describe the deviations from the idealized Eshelby picture observed at the particle scale, and the sensitivity of their predictions to such microscopic details should be examined.

ACKNOWLEDGMENTS

We thank Jean-Louis Barrat for discussions related to this study. J.R. was supported by the Discovery Grant Program of the Natural Sciences and Engineering Research Council of Canada. This research was supported in part by the National Science Foundation under Grant No. NSF PHY11-25915.

[1] A. Argon and H. Kuo, Mater. Sci. Eng. **39**, 101 (1979).
[2] M. L. Falk and J. S. Langer, Phys. Rev. E **57**, 7192 (1998).
[3] C. E. Maloney and A. Lemaître, Phys. Rev. E **74**, 016118 (2006).
[4] K. W. Desmond and E. R. Weeks, Phys. Rev. Lett. **115**, 098302 (2015).
[5] J.-C. Baret, D. Vandembroucq, and S. Roux, Phys. Rev. Lett. **89**, 195506 (2002).
[6] J. Antonaglia, W. J. Wright, X. Gu, R. R. Byer, T. C. Hufnagel, M. LeBlanc, J. T. Uhl, and K. A. Dahmen, Phys. Rev. Lett. **112**, 155501 (2014).
[7] A. Nicolas, E. E. Ferrero, K. Martens, and J.-L. Barrat, arXiv:1708.09194.
[8] J. Eshelby, Proc. R. Soc. A **241**, 376 (1957).
[9] F. Puosi, J. Rottler, and J.-L. Barrat, Phys. Rev. E **89**, 042302 (2014).
[10] A. Nicolas, K. Martens, L. Bocquet, and J.-L. Barrat, Soft Matter **10**, 4648 (2014).
[11] S. Sandfeld and M. Zaiser, J. Stat. Mech.: Theor. Exp. (2014) P03014.
[12] M. Talamali, V. Petäjä, D. Vandembroucq, and S. Roux, Phys. Rev. E **84**, 016115 (2011).
[13] Z. Budrikis and S. Zapperi, Phys. Rev. E **88**, 062403 (2013).
[14] E. Homer and C. Schuh, Acta Mater. **57**, 2823 (2009).
[15] P. Schall, D. Weitz, and F. Spaepen, Science (NY) **318**, 1895 (2007).
[16] Y. Ma, J. Ye, G. Peng, D. Wen, and T. Zhang, Mater. Sci. Eng.: A **627**, 153 (2015).
[17] T. Albaret, A. Tanguy, F. Boioli, and D. Rodney, Phys. Rev. E **93**, 053002 (2016).
[18] A. Nicolas, J. Rottler, and J.-L. Barrat, Eur. Phys. J. E **37**, 50 (2014).
[19] A. Lemaître, J. Chem. Phys. **143**, 164515 (2015).
[20] H. Schwarz, Recl. Trav. Chim. **84**, 771 (1965).
[21] H. Princen, J. Colloid Interface Sci. **91**, 160 (1983).
[22] A.-L. Biance, A. Calbry-Muzyka, R. Höhler, and S. Cohen-Addad, Langmuir **28**, 111 (2011).
[23] I.-C. Choi, Y. Zhao, Y.-J. Kim, B.-G. Yoo, J.-Y. Suh, U. Ramamurty, and J.-i. Jang, Acta Mater. **60**, 6862 (2012).
[24] F. Boioli, T. Albaret, and D. Rodney, Phys. Rev. E **95**, 033005 (2017).
[25] A. Nicolas, J.-L. Barrat, and J. Rottler, Phys. Rev. Lett. **116**, 058303 (2016).
[26] V. Chikkadi and P. Schall, Phys. Rev. E **85**, 031402 (2012).
[27] X. Jin, X. Zhang, P. Li, Z. Xu, Y. Hu, and L. M. Keer, J. Appl. Mech. **84**, 074501 (2017).

[28] A. Nicolas, The Flow of Amorphous Solids: Elastoplastic Models and Mode-Coupling Approach, Ph.D. thesis, Université de Grenoble, 2014.

[29] Incidentally, note that this is much less the case if STs are binned according to $\theta^{\mathrm{pl}}_{\mathrm{Loc}}$.

[30] S. Patinet, D. Vandembroucq, and M. L. Falk, Phys. Rev. Lett **117**, 045501 (2016).

[31] A. Barbot, M. Lerbinger, A. Hernandez-Garcia, R. García-García, M. L. Falk, D. Vandembroucq, and S. Patinet, Phys. Rev. E **97**, 033001 (2018).